British Journal of Applied Science & Technology
4(6): 945-966, 2014

SCIENCEDOMAIN *international*
www.sciencedomain.org

Component-based Thermal Face Recognition

Naser Zaeri[1*]

[1]*Faculty of Computer Studies, Arab Open University, P.O. Box 3322, Safat 13033, Kuwait.*

Author's contribution

This Whole work was carried out by the author NZ.

Original Research Article

Received 7th August 2013
Accepted 3rd December 2013
Published 27th December 2013

ABSTRACT

Face recognition based only on the visible spectrum has shown difficulties in performing consistently in uncontrolled operating conditions. Face recognition using different imaging modalities, particularly infrared imaging sensors has become an area of growing interest in recent years. In this paper, we present a new technique for face recognition that exploits the local statistical characteristics of a thermal image. The "whole" face image is divided into components of different sizes. The statistical features of these components, beside the "whole" image are combined together using fusion methods. Decision level fusion finds a combination of multiple statistical patterns to produce an integrated result that is enhanced in terms of information content for pattern recognition and classification. Local representations offer robustness against variability due to the changes in localized regions of the objects. The proposed feature vector consists of different moments' calculations and thermal components' histograms. The features found from local analysis are less sensitive to illumination changes, easier for estimating the rotations, have less computational burden and have the potential to achieve higher correct recognition rates. The experimental results reveal that the new system can achieve a success rate of 96.4% when implemented on the AIAOU Database.

Keywords: Face recognition; thermal image; feature extraction; histogram distribution.

1. INTRODUCTION

Research into several biometric modalities, including face, fingerprint, iris and retina recognition has produced varying degrees of success [1]. Face recognition stands as the

**Corresponding author: E-mail: n.zaeri@aou.edu.kw;*

most appealing modality, since it is the natural mode of identification among humans and does not need to interrupt user activities. Despite successes in indoor access control applications, imaging in the visible spectrum demonstrates difficulties in recognizing the faces in conditions of varying illumination, especially under total darkness conditions [2]. Face recognition based only on the visible spectrum has shown difficulties in performing consistently in uncontrolled operating conditions [3]. Since the face is essentially a three-dimensional object, lighting sources from different directions may significantly change visual appearances. Light reflected from human faces also varies depending on the skin colour of people from different ethnic groups. This variability, coupled with dynamic lighting conditions, may cause great difficulties in recognizing the face in applications such as outdoor surveillance tasks.

Face recognition using different imaging modalities, particularly infrared (IR) imaging sensors has become an area of growing interest [4,5]. The use of thermal IR images can improve the performance of face recognition in uncontrolled illumination conditions [6]. IR cameras provide a measure of thermal emissivity from the facial surface and their images are relatively stable under illumination variation. The anatomical information which is imaged by infrared technology involves subsurface features believed to be unique to each person [2], though the twin's images are not necessarily substantially different. These features may be imaged at a distance using passive infrared sensor technology, with or without the cooperation of the subject. The other advantage is that it is very difficult to alter this information purposefully. The thermal IR spectrum that comprises mid-wave IR (3–5 μm) and long-wave IR (8–12 μm) bands is used as a source of information for face detection and recognition. Thermal IR sensors measure the heat energy that is emitted, not reflected, from the object. IR energy can be viewed in any light conditions and is less subject to scattering and absorption by smoke or dust than visible light.

In this paper, we present a new technique for face recognition that exploits the local characteristics of the thermal image. The "whole" face image is divided into components of different sizes. The statistical features of these components, beside the "whole" image are combined using fusion methods. Decision-level fusion finds a combination of multiple statistical patterns to produce an integrated result that is enhanced in terms of information content for pattern recognition and classification. Local representations offer robustness against variability due to the changes in localized regions of the objects. The features used in the local feature analysis methods are less sensitive to illumination changes, easier for estimating the rotations and have less computational burden. Hence, the proposed system employs the advantages and the characteristics of thermal images, component-based approach, the statistical features and fusion. The evaluation used a database of thermal IR face images that has been recently developed by the Artificial Intelligence laboratory at the Arab Open University (AIAOU Database) [7]. Our work makes the following contributions: First, it proposes a way to achieve thermal face image representation in a simple manner. Second, it utilizes the statistical characteristics of thermal components alongside the advantages of results fusion. Third, it provides a large number of experimental results that show that the proposed method is good enough to recognize a person in a competitive way, especially when considering consumed time and speed. The organization of the paper is as follows. A brief literature review is given in Section 2. Section 3 discusses the proposed new method. A brief description of the system is given in Section 4. The experimental results and analysis are discussed in Section 5. Finally, the paper is brought to a conclusion in Section 6.

2. LITERATURE REVIEW

In thermal imagery of human tissue, the major blood vessels have weak sigmoid edges. This is due to the natural phenomenon of heat diffusion, which means that when two objects with different temperatures are in contact (e.g. vessel and surrounding tissue), heat conduction creates a smooth temperature gradient at the common boundary [8]. Due to its physiology, a human face consists of “hot” parts that correspond to tissue areas that are rich in vasculature and “cold” parts that correspond to tissue areas with sparse vasculature. Every living and non-living object at a finite temperature emits radiation, which can be captured by infrared cameras. Early studies by Socolinsky et al. in [9,10,11] suggest that long-wave infrared imagery of human faces is not only a valid biometric, but superior to using comparable visible-light imagery. However, the testing set size in these studies is relatively small, the training and gallery are composed of disjoint sets of images of the same subjects, and there is no substantial time lapse between gallery and probe image acquisition. Prokoski et al. [5] anticipated the possibility of extracting the vascular network from thermal facial images and using it as a feature space for face recognition. However, they did not present an algorithmic approach for achieving this. Authors in [12] proposed an approach using wide-baseline matching of face vascular networks obtained from thermal images. The vascular networks are obtained through skin segmentation and morphological operators. The image matching stage uses SIFT descriptors for verifying correspondences and generating a final geometrical transformation that relates the vascular networks. However, the proposed skin detection model is created by modelling the skin pixel intensity distribution of non-skin intensity distribution as mixture of Gaussians. This is a time- and memory-consuming task. Furthermore, the general parameters for the Gaussians cannot be obtained, as they depend on the response of the particular camera to thermal intensity. The authors have reported a best recognition rate of 95.7% for a small database that consists of 156 thermal images. A combination of principal component analysis technique and a Bayesian Maximum Likelihood for thermal face image classification was proposed in [13]. The Bayesian approach uses a probabilistic measure of similarity based on a Bayesian Maximum Likelihood analysis of image differences. In this work authors have developed nonlinear technique for multispectral face recognition. However, most of the obtained results were poor. Bayesian face recognition needs a sufficient number of face images for intrapersonal learning process and if the number of these images is low then the system performance will be inefficient.

Bhowmik et al. [14] introduced the role of different IR spectrums and their applications. In their experimental work, they fused both thermal and visible images to enhance the recognition rate, as it is expected that the fusion process improves the overall performance of the system. They tested their method on IRIS and Terravic databases. The images of both databases were taken in one session. In other words, the effect of time lapse was not taken into consideration. Lu et al. [15] conducted a study on normalization of infrared facial images, especially those resulting from variant ambient temperatures. Three normalization methods were proposed to eliminate this effect. The experimental results showed that the proposed methods can increase the robustness of infrared face recognition system and greatly improve its performance on time-lapse data. They recorded a maximum success rate of 89.1% using PCA with weigh coefficient. Huang et al. [16] proposed a method called discriminative spectral regression to map face images from various modalities, such as the visual, the IR modality and the sketch modality into a common discriminative subspace. They introduced two regularization terms, which reflect the category relationships among data, into the least squares approach where the class information is integrated in the cost function. However, the method does not make sufficient use of the discriminative information

among the images from different classes. Its performance can be further improved by introducing the category relationship into its objective function. In addition, the proposed variation of the optimization problem is computationally exhaustive. Nicolo and Schmid [17] presented a cross-spectral face recognition scheme that encodes images filtered with a bank of Gabor filters followed by three local operators: Simplified Weber Local Descriptor, Local Binary Pattern, and Generalized Local Binary Pattern. Both magnitude and phase of filtered images are encoded. The proposed technique can be used in challenging atmospheric conditions such as rain and mist. Also, it is applicable to scenarios where no IR data are available for training the system. However, the authors did not discuss how the filter parameters were chosen.

Guzman et al. [18] discussed a thermal imaging framework that consolidates the steps of feature extraction through the use of morphological operators and registration using the linear image registration tool. The matching showed an average accuracy of 88.46% for skeletonized signatures and 90.39% for isotropically diffused signatures. Poursaberi et al. [19] developed a concept for decision-making support in biometric-based situational awareness systems. Such systems assist users in gathering and analysing biometric data, and support the decision-making on the human behavioural pattern and/or authentication. As an example, the authors consider a facial biometric assistant that functions based on multi-spectral biometrics in visible and infrared bands. Seal et al. [20] proposed a human face recognition system based on wavelet transform from thermal IR images. Their method utilizes a “Haar” wavelet to extract a low frequency band from the cropped face region, and the classification is based only on low-frequency components. In general, wavelet transform captures both frequency and time (location information). Haar transformation was used because of its simplicity. However, the proposed method in [20] ignores details at different levels, some of which might be of great importance, especially if they contain important discriminant features. The same authors have proposed another work on thermal face recognition based on the use of minutiae points [21]. They suggested that there is an analogy between thermal imprints of human faces and fingerprints of human beings. Thermal imprints of blood vessels may be treated as ridges in fingerprints, and fingerprint recognition techniques may be applied to the thermal imprints of the human faces in order to recognize them. In this work they used three methods to extract the blood perfusion image: bit-plane slicing, morphological erosion and Sobel edge operators. The computational complexity of the proposed work is relatively large and can be exhaustive if applied on large databases. Authors in [22] proposed using a local binary pattern (LBP) for thermal face recognition. Multilayer feed forward neural network and minimum distance classifier were used to classify face images. The maximum success rate they obtained was ~95% when tested on a locally generated database consisting of 578 images. However, this system is applicable only to front views with constant background. It may fail in unconstrained environments like natural scenes.

On the other hand, at the level of component-based face recognition techniques, authors in [23] demonstrated two local nonlinear techniques for face recognition: Linear Graph Embedding and Locality Preserving Projection. These techniques find an embedding that preserves local information. The aim was to represent the data in a lower dimensional subspace while preserving the local structure of the original image space. They have recorded a best recognition rate of 91%. However, their proposed techniques are computationally greedy. Tongzhou et al. [24] divided each original image sample into a certain number of sub images, where all the training sub images from the same position constructed a series of new training sub-pattern sets, and the PCA followed by Gabor wavelet were used to extract local projection sub-feature vectors to obtain a set of projection

sub-spaces. Zaeri et al. [25] have applied a component-based linear discriminant analysis approach to systems requiring high-speed performance. The proposed method enhanced the performance of the system and achieved high recognition rates. Recently, a number of learning methods using local transform sparse representation have been proposed in visible spectrum. Xu et al. [26] and Xu et al. [27] have proposed a two-phase test sample sparse representation method. The first phase seeks to represent the test sample as a linear combination of all the training samples and exploits the representation ability of each training sample to determine *M* "nearest neighbours" for the test sample. The second phase represents the test sample as a linear combination of the determined *M* nearest neighbours and uses the representation result to perform classification. Similarly, Yang et al. [28] has focused on sparse representation based classification, where they gave a theoretical justification to support the effectiveness of sparse representation-based classifiers. Also, we have recently discussed the feasibility of a new method for face recognition in visible spectrum at the component level [29]. Motivated by the abovementioned discussion and by the results we have obtained from our previous work in the visible spectrum, we propose a new face recognition system that exploits the advantages and characteristics of both the thermal images approach and the component-based approach.

3. THERMAL IMAGE HISTOGRAM

The histogram of a thermal image (similar to a digital one) with temperature levels in the range [0, *L*–1] is a discrete function $h(r_k) = n_k$, where r_k is the k^{th} temperature value and n_k is the number of "pixels" in the image with temperature r_k. The histogram can be normalized by dividing each of its components by the total number of pixels in the image, denoted by the product *MN*, where *M* and *N* are the row and column dimensions of the image. Thus, a normalized histogram is given by

$$H = p(r_k) = n_k/MN, \text{ for } k = 0, 1, 2, \ldots, L - 1. \quad (1)$$

It is common to consider $p(r_k)$ as an estimate of the probability of the occurrence of temperature level r_k in an image. A plot of $p_r(r_k)$ versus r_k is commonly referred to as a "histogram" or histogram distribution. Histograms provide useful image statistics with distinctive features that can be used for face image recognition. Further, they are simple to calculate in software and also lend themselves to economic hardware implementations, thus making them a popular tool for real-time face recognition.

Moreover, if we let *r* denote a discrete random variable representing temperature values in the range (0, *L*–1) and if we let $p(r_k)$ denote the normalized histogram component corresponding to value r_k, the *n*th moment of *r* about its mean is defined as

$$\mu_n(r) = \sum_{i=0}^{L-1} (r_i - \mu)^n p(r_i) \quad (2)$$

where μ is the mean (average temperature) value of *r*

$$\mu = \sum_{i=0}^{L-1} r_i p(r_i) \quad (3)$$

This is an important image feature that can be considered as an element in the feature vector that represents the "centre of gravity" of the face temperature distribution. Another important feature to be considered is the spread of these temperature values across the face image. This is given by the variance (or standard deviation) of this set, which can be obtained from the second moment.

$$\sigma^2 = \mu_2(r) = \sum_{i=0}^{L-1} (r_i - \mu)^2 p(r_i) \quad (4)$$

In this paper, we propose a feature vector that consists of the following different feature parameters: first moment, second moment and the thermal image histogram. The calculation of the first and second moments and the histogram distribution is implemented at the component level, beside the whole face image. The final decision results depend on the *local* mean, variance and histogram beside the computation of the *global* mean, variance and histogram over the entire thermal face image. These local parameters are more powerful in preserving the discriminant features in a neighbourhood of a pixel in an image.

If (*x*, *y*) denote the coordinates of any pixel in a given image, and if S_{xy} denotes a neighbourhood (component) of a specified size, centred on (*x*, *y*), then the mean value of the pixels in this neighbourhood is given by

$$\mu_{S_{xy}} = \sum_{i=0}^{L-1} r_i p_{S_{xy}}(r_i) \quad (5)$$

where $p_{S_{xy}}$ is the histogram of the pixels in region S_{xy}. Similarly, the variance of the pixels in the neighbourhood is given by

$$\sigma^2_{S_{xy}} = \sum_{i=0}^{L-1} \left(r_i - \mu_{S_{xy}}\right)^2 p_{S_{xy}}(r_i) \quad (6)$$

As before, the local mean is a measure of average temperature in neighbourhood S_{xy} and the local variance is a measure of temperature spread in that neighbourhood.

We propose the following scheme in dividing the face image:

a) First, we take the whole image as one component. We denote this component as f_0
b) Second, we take only the centre part of the face that consists of the eyes, nose and mouth. We denote this component of the face as f_1^0
c) Third, we divide the thermal image into four different equal-sized components and denote them as $f_2^0, f_2^1, f_2^2, f_2^3$
d) Fourth, we divide the thermal image into 16 different equal-sized components and denote them as $f_3^0, f_3^1, f_3^2, \ldots, f_3^{15}$

Then, we find the average temperature, the variance and the histogram distribution for every component as described above. Finally, the feature vector for every component is formed as follows:

$$f_i^j = [\mu_i^j, {\sigma^2}_i^j, H_i^j]^T \quad (7)$$

Where *T* denotes the transpose, μ_i^j is the average temperature for the corresponding component as defined in equation (5) and ${\sigma^2}_i^j$ is the corresponding variance as defined in equation (6). H_i^j is defined by equation (1). The Euclidean distance (L_2 norm) is used as the system classifier and is given by

$$D(\mathbf{a}, \mathbf{b}) = \left(\sum_{k=1}^{d} (a_k - b_k)^2 \right)^{1/2} \quad (8)$$

for vectors **a** and **b** both of *d* dimensions.

The results obtained from the similarity measures from the feature vectors for the different number of components are fused together to achieve the final similarity score. Decision-level fusion combines the results to yield a final fused decision based on a joint assertion of multiple single source results (or decisions) to achieve an improved classification. Prior knowledge and domain-specific information can also be incorporated. Fusion techniques exploit synergistic integration of the information obtained from different data sources or from multiple pattern classifiers to produce a more detailed form than the original and hence improve the overall classification accuracy [30]. Fusion methods include AND fusion, OR fusion, majority voting and ranked list combination. In our experiments, we have implemented AND fusion, as it has proven its superiority among the other fusion methods. It is worth mentioning that the study of best fusion method is beyond the scope of this paper. Fig. 1 details the proposed technique.

4. SYSTEM DESCRIPTION AND SETUP

To capture the thermal images, we used the Infrared Camera ETIP 7320 (Fig. 2) which includes a state-of-the-art thermal infrared imaging radiometer. The core technology used in the system is a sophisticated thermal imaging technology using a micro-bolometer 320×240 focal plane array and a Vanadium Oxide technology base, ensuring very high efficient thermal and spatial resolution.

We have built a database of 570 images for 19 different subjects taken in different sessions. The database consists of males and females from various ethnic backgrounds. Acquisitions were held at different times and most subjects participated in multiple sessions across a number of different weeks. Infrared images were acquired in the 7.0–14.0 μm range and consist of an un-cooled focal plane array incorporating a 320×240 matrix of microbolometer detectors. Examples of thermal images from the AIAOU database for different subjects are shown in Fig. 3. Each face-recognition experiment is characterized by three image sets:

a) The training set: used to form a face space in which the recognition is performed. This set consists of five images per subject (class). These images were chosen randomly among the 30 available images for each subject.
b) The gallery set: contains the set of ‘‘enrolled’’ images of the subjects to be recognized and each image is uniquely associated with the identification of a distinct subject in the set. This set also consists of five images per subject and were similarly chosen randomly among the 30 available images for each subject.

c) The probe (testing) set: is a set of images to be identified via matching against the gallery. This set consists of 380 images (20 images per subject × 19 subjects).

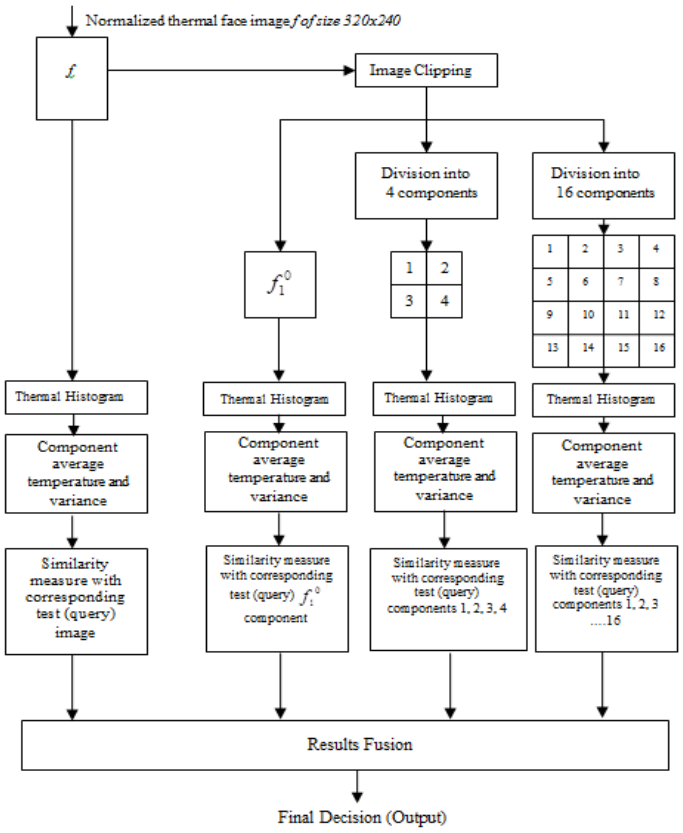

Fig. 1. The proposed new technique

Fig. 2. Infrared camera ETIP 7320

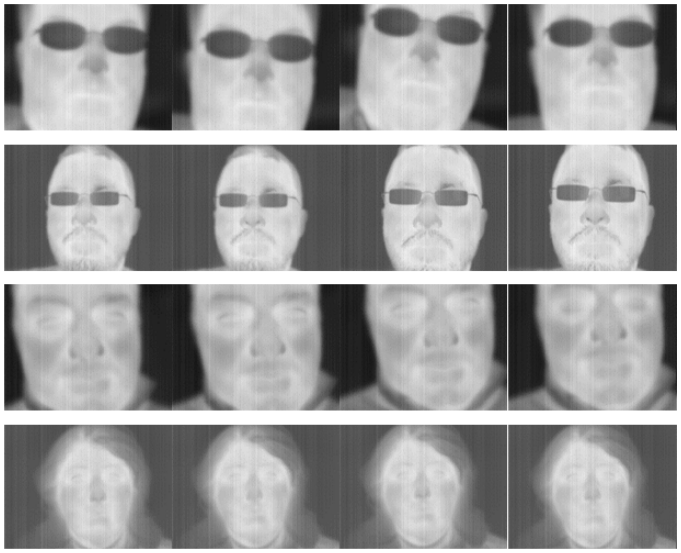

Fig. 3. Examples of thermal images from the AIAOU database for different subjects

5. EXPERIMENTAL RESULTS AND ANALYSIS

Before conducting our experiments, we took several pre-processing steps:

a) Integer to float conversion: After the image is read from a file, it is converted to double precision floating point for subsequent image calculations.
b) Geometric normalization: This aligns images such that the faces are the same size, in the same position and at the same orientation. Specifically, the image is scaled and rotated to make the eye coordinates coincident with pre-specified locations in the output.
c) Masking: This is used to eliminate less important parts of the image, ensuring that the face-recognition system does not respond to features corresponding to background, hair, clothing, etc.

Table 1(a) shows skin mean temperature over each block of the different blocks described in Fig. 1 for five different images belonging to the same subject (person). Table 1(b) shows the corresponding values for another person. Similar results are recorded in Table 2 for temperature variance.

Table 1. Skin mean temperature (in degrees Celsius) for each block for different images: (a) of the same person and (b) of another person

(a)

	Image 1	Image 2	Image 3	Image 4	Image 5
f_1^0	29.0	29.9	29.1	30.7	30.4
f_2^0	22.9	24.1	28.0	26.0	24.9
f_2^1	23.5	24.2	28.0	26.0	25.1
f_2^2	25.7	27.3	23.6	25.4	25.5
f_2^3	26.7	27.8	23.8	25.7	26.3
f_3^0	19.6	19.7	24.3	21.1	19.8
f_3^1	19.9	20.0	26.0	22.3	20.6
f_3^2	20.2	20.3	25.3	21.9	20.9
f_3^3	20.8	20.6	24.5	21.7	20.4
f_3^4	24.7	27.6	30.8	29.9	28.7
f_3^5	27.5	29.0	31.0	30.7	30.4
f_3^6	27.3	29.1	31.1	30.6	30.3
f_3^7	25.5	26.7	31.2	29.9	28.6
f_3^8	28.9	30.6	25.6	29.3	29.1
f_3^9	30.5	30.7	27.2	30.7	30.5
f_3^{10}	30.8	30.9	27.0	30.9	30.6
f_3^{11}	30.8	31.2	25.6	29.4	30.9
f_3^{12}	20.8	23.0	20.6	20.6	20.5
f_3^{13}	22.7	24.8	20.9	21.2	21.8
f_3^{14}	22.8	25.1	21.1	21.3	22.4
f_3^{15}	22.4	23.8	21.3	21.5	21.4

(b)

	Image 1	Image 2	Image 3	Image 4	Image 5
f_1^0	28.3	30.0	30.7	28.3	29.3
f_2^0	26.8	25.3	25.6	26.1	26.5
f_2^1	28.6	27.1	29.6	28.8	29.3
f_2^2	26.5	25.5	25.5	25.1	24.9
f_2^3	29.5	28.0	26.3	26.5	26.3
f_3^0	27.7	22.7	22.3	24.3	24.7
f_3^1	22.3	23.0	24.9	24.1	25.8
f_3^2	25.9	22.1	26.0	25.2	25.5
f_3^3	24.9	22.8	28.1	26.3	27.8
f_3^4	31.5	27.1	24.5	30.4	28.0
f_3^5	25.9	28.3	30.6	25.6	27.4
f_3^6	31.0	31.7	32.1	31.3	31.8
f_3^7	32.6	31.9	32.1	32.4	32.3
f_3^8	30.8	28.9	27.4	31.4	29.9
f_3^9	25.7	28.4	28.9	25.8	27.2
f_3^{10}	30.7	31.7	31.5	30.5	31.1
f_3^{11}	32.4	32.1	31.5	32.0	32.0
f_3^{12}	25.8	22.2	23.1	22.8	21.9
f_3^{13}	23.6	22.6	22.7	20.5	20.6
f_3^{14}	26.9	24.4	22.1	22.4	22.1
f_3^{15}	28.2	23.8	20.0	21.1	20.1

Table 2. Skin temperature variance for each block for different images: (a) of the same person and (b) of another person

(a)

	Image 1	Image 2	Image 3	Image 4	Image 5
f_1^0	12.60	6.01	13.80	1.29	0.95
f_2^0	21.73	25.28	19.04	24.15	27.14
f_2^1	19.50	22.93	18.62	22.92	25.99
f_2^2	23.89	21.36	18.96	24.59	24.35
f_2^3	22.18	20.02	16.20	22.67	23.35
f_3^0	0.22	0.23	18.69	3.65	1.50
f_3^1	0.21	0.22	21.83	11.69	4.85
f_3^2	0.26	0.26	19.13	7.65	6.81
f_3^3	0.69	0.32	15.17	1.56	0.27
f_3^4	23.61	18.40	0.43	5.30	12.42
f_3^5	18.76	10.16	0.83	0.98	0.97
f_3^6	18.19	7.63	0.61	1.56	1.16
f_3^7	22.26	24.13	0.46	9.19	17.56
f_3^8	8.85	0.21	23.37	10.78	9.32
f_3^9	0.92	0.95	19.31	1.03	0.88
f_3^{10}	0.45	0.31	19.19	1.30	0.57
f_3^{11}	0.40	0.31	17.99	10.42	0.51
f_3^{12}	4.53	16.60	0.23	0.38	1.79
f_3^{13}	14.33	20.46	0.22	1.32	8.89
f_3^{14}	13.11	17.82	0.19	1.20	10.84
f_3^{15}	7.95	17.10	0.26	0.39	3.55

(b)

	Image 1	Image 2	Image 3	Image 4	Image 5
f_1^0	5.8	5.8	9.2	9.7	6.0
f_2^0	12.6	12.7	15.4	15.5	17.9
f_2^1	10.6	11.6	14.1	14.1	15.4
f_2^2	11.6	11.5	13.0	12.8	13.2
f_2^3	13.9	14.3	14.0	12.7	14.6
f_3^0	16.6	17.0	0.3	0.2	7.6
f_3^1	9.1	10.2	0.2	0.2	8.9
f_3^2	16.1	15.7	0.2	0.4	4.0
f_3^3	6.7	7.5	3.8	3.9	3.9
f_3^4	0.2	0.2	12.3	9.5	1.3
f_3^5	5.7	5.6	9.1	9.0	4.7
f_3^6	0.9	1.3	13.0	13.0	7.1
f_3^7	0.6	0.6	9.9	10.0	2.2
f_3^8	4.8	6.3	4.2	0.2	3.4
f_3^9	6.5	6.5	5.3	7.2	6.0
f_3^{10}	4.6	4.3	5.7	1.1	6.3
f_3^{11}	8.5	8.7	2.0	0.5	2.3
f_3^{12}	0.2	0.2	1.8	8.5	0.8
f_3^{13}	0.6	0.4	7.8	11.5	4.9
f_3^{14}	0.3	0.3	8.6	13.3	6.6
f_3^{15}	6.3	5.8	4.6	5.5	4.9

Fig. 4 shows histogram distribution of a whole face image for one subject (class) for different number of bins: 20, 50, 100, 200, 300, 400, and 500 bins. Fig. 5 shows the corresponding histograms for another subject. The distinctive and discriminant features between the two figures (subjects) are obvious.

In Fig. 6, we show the histogram distribution for four different images for the same person (same class) in the case of 20 bins. As can be seen from the figure, the general characteristics of all four histograms are similar. Hence, the discriminant features within the class are preserved. Fig. 7 shows the histogram distribution for another four different images of another person (class) in the case of 100 bins. Again, this figure shows that the discriminant features for the same class (person) are preserved among the four images. This supports the concept of utilizing this statistical measure as a human identification method.

To further support this idea, we show in Fig. 8 the histogram distribution for 10 different persons where each distribution corresponds to a different person (class) for the case of 20 bins. Similarly, Fig. 9 shows the results for the case of 100 bins. As we can see from Figs 8 and 9, the discriminant features between classes (that is for different persons) are remarkable and every class can be characterized by its own discriminant features.

In order to justify the implementation of the method at the component level, we need to analyse the local statistical characteristics for a thermal image. Fig. 10 shows a thermal image for one subject and the corresponding temperature distribution over the entire face. The temperature variations can be clearly seen over the different parts of the face. This shows that these parts have different thermal characteristics, giving the human face its own thermal identity. We take a further step in our analysis and show the thermal statistical features of the centre part of the face, f_1^0. The local distinctive features are obvious in Fig. 11. Similar observation can be obtained when investigating the four thermal components $f_2^0, f_2^1, f_2^2, f_2^3$ shown in Fig. 12. More distinctive features of thermal face components can be found in Fig. 13 when we analyse the 16 components $f_3^0, f_3^1, f_3^2, \dots, f_3^{15}$. Fig. 14 shows the histogram distribution for components $f_3^0, f_3^1, f_3^2, \dots, f_3^{15}$ corresponding to Fig. 13(b). Figs. 11 to 14 justify our rationale for using local thermal features for human identification.

The recognition rates for the different number of bins are recorded in Fig. 15. As can be seen from the figure, the rank-1 recognition rate was at its lowest when the number of bins was 20, with a success rate of 85.2%. The recognition rate increased as the number of bins increased and reached 96.4% when there were 500 bins. We have noticed that the success rate saturates as the number of bins becomes greater than 500. Another method to evaluate the potential performance of the recognition system is the Cumulative Match Score curve (CMS). The CMS illustrates the trade-off of true positive versus false positive results. The Y-axis represents the true positive rate, and the X-axis is the cumulative rank. We can think of the X-axis as the maximum number of images that the system is allowed to report when giving an alarm for a given probe. If the system is allowed to report a larger number of possible matches, the true positive rate generally increases. The results of the CMS evaluation are shown in Fig. 16, where the performance statistics are reported as cumulative match scores. Identification is regarded as correct if the true object is in the top Rank *n* matches, with Rank 1 being the best match.

For the sake of comparison, we show in Table 3 experimental results with thermal images obtained by different researchers. It should be noted that the databases used by researchers in the mentioned works are not the same. This is to be expected since this field of study is

relatively new when compared to face recognition in visible spectrum, and the community has not yet reached a general agreement on standard tests or benchmark databases.

An important advantage of our system is its speed and efficiency. Table 4 shows the time consumed by the system to complete the histogram calculations for different components. As can be seen from Tables 3 and 4, the system performance demonstrates its effectiveness when both the recognition rate and the time consumed are considered.

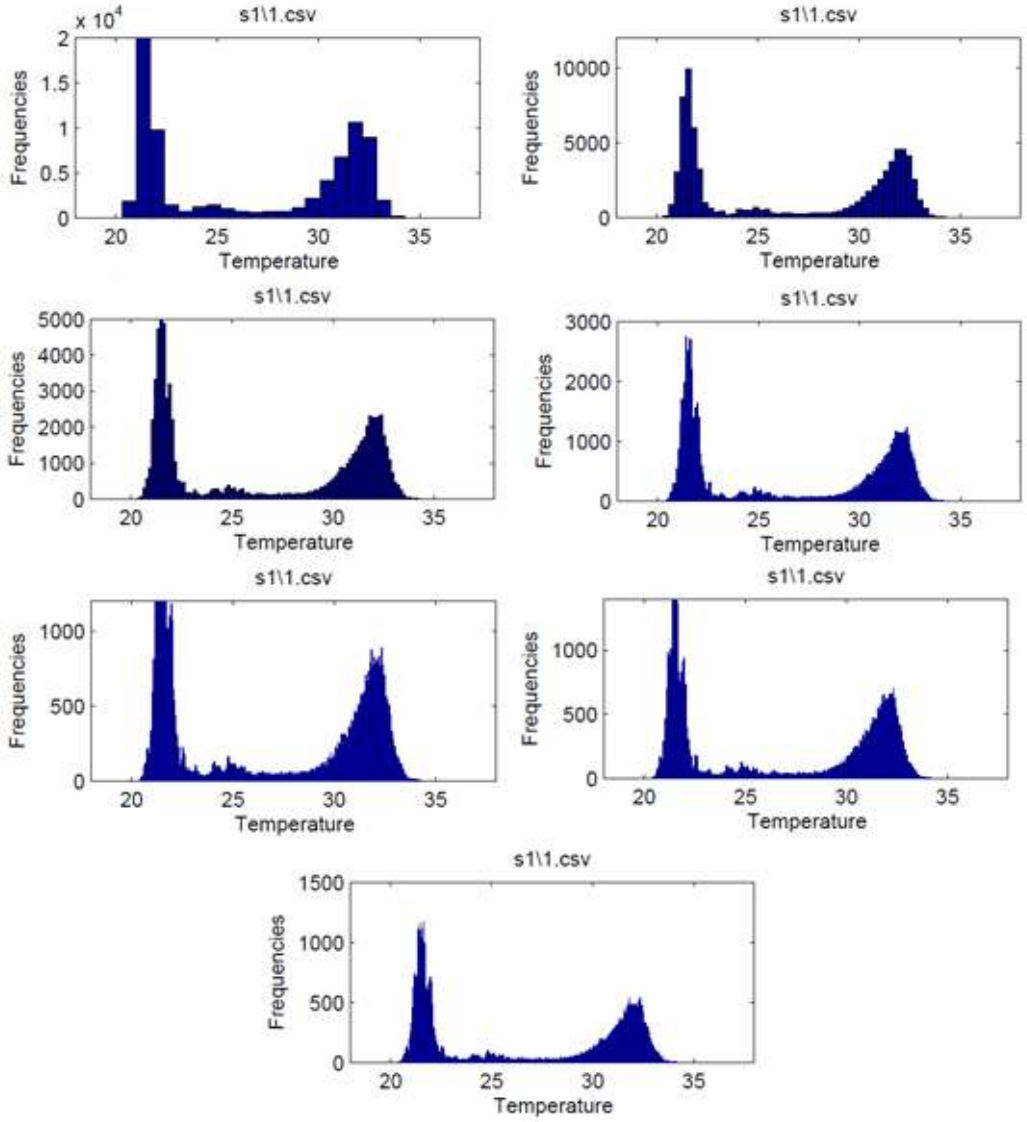

Fig. 4. Histogram distribution for a whole face image for one subject (class) for different number of bins: 20, 50, 100, 200, 300, 400 and 500 bins

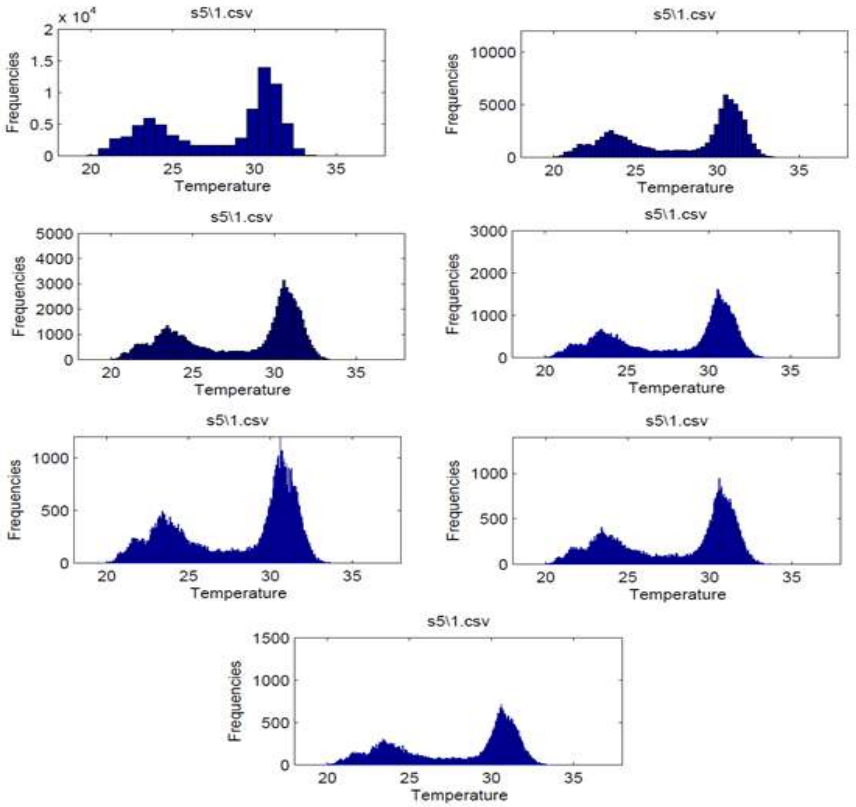

Fig. 5. Histogram distribution for a whole face image for another subject (class) for the same number of bins as described in Fig. 4

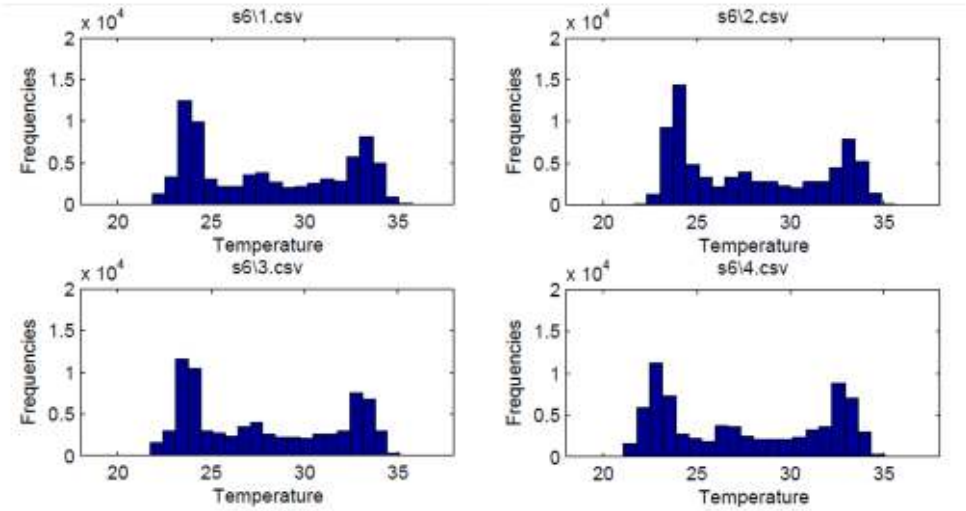

Fig. 6. Histogram distribution for four different images for the same person (same class) in the case of 20 bins

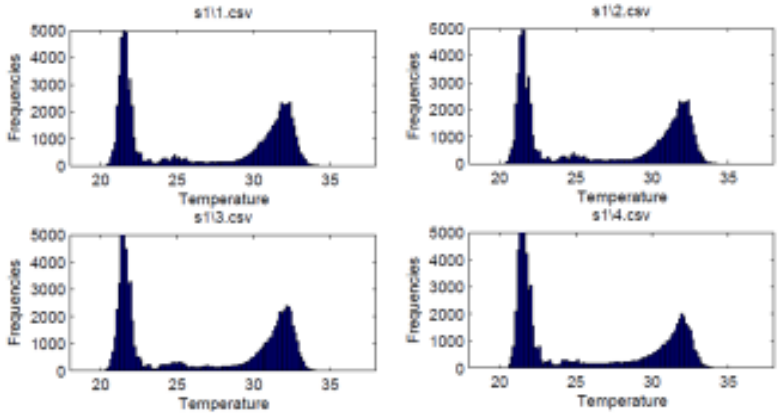

Fig. 7. Histogram distribution for another four different images for another person (class) in the case of 100 bins

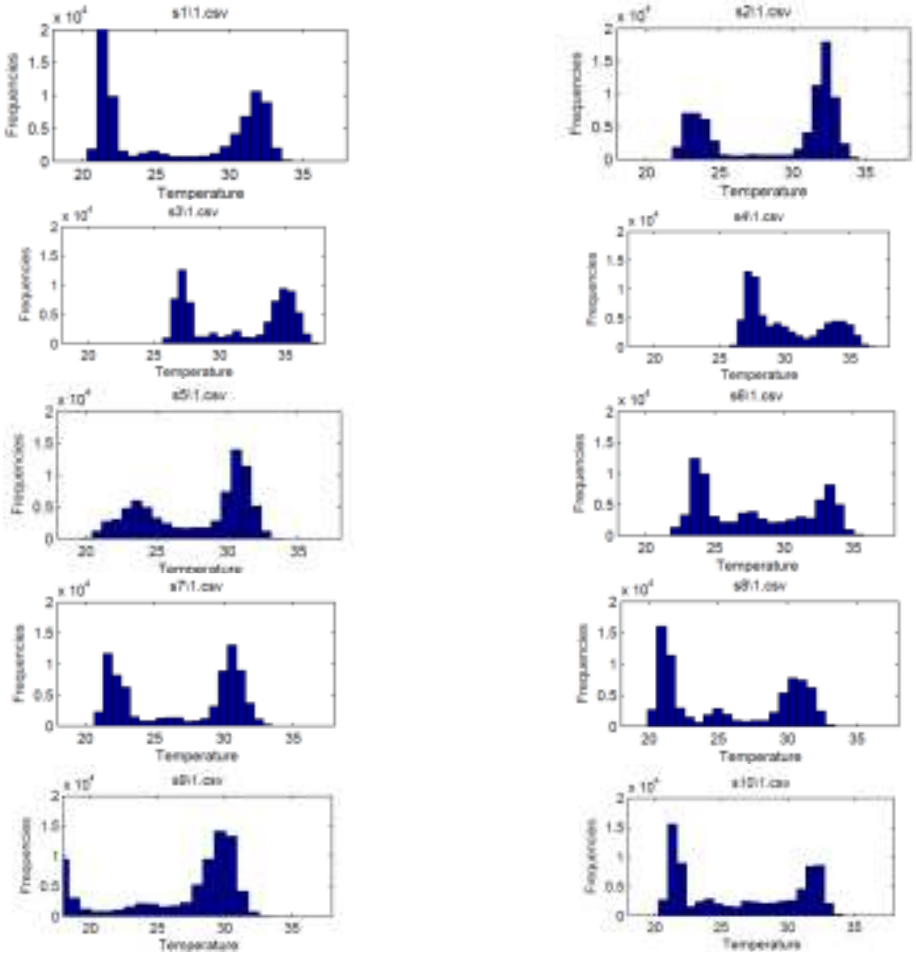

Fig. 8. Histogram distribution for 10 different persons in the case of 20 bins

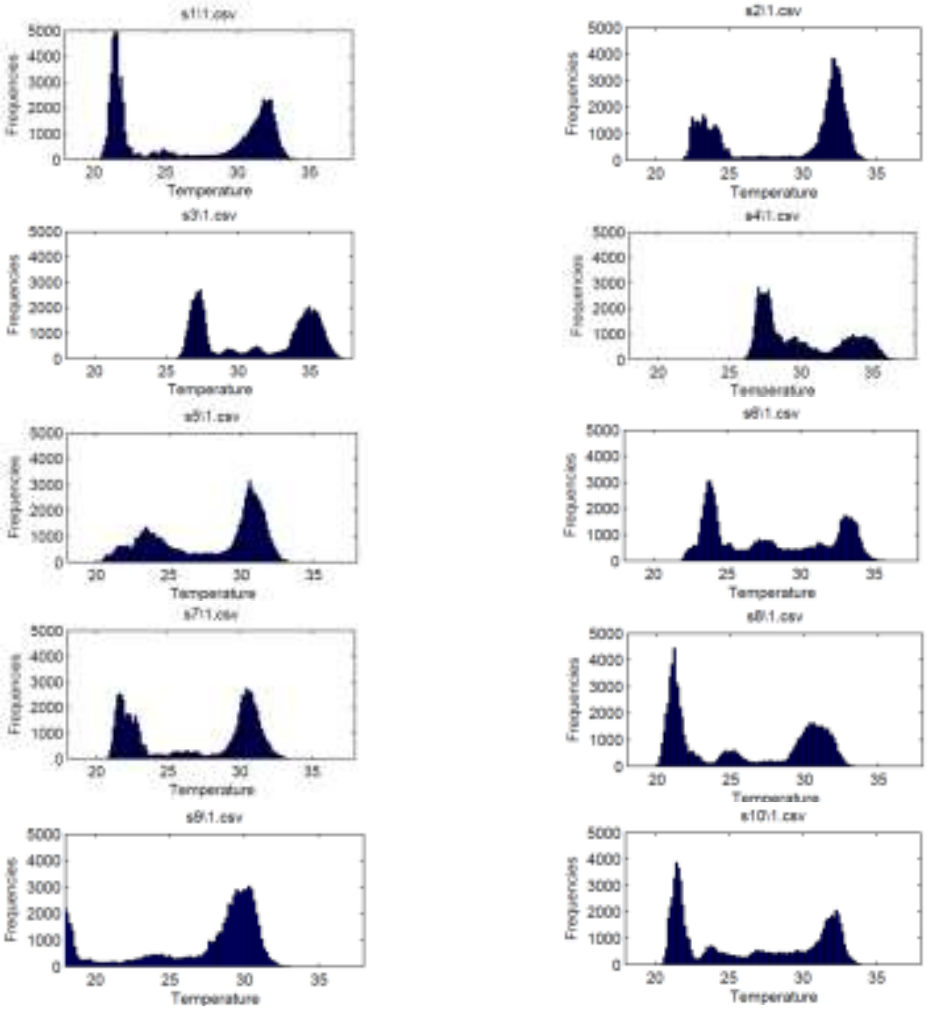

Fig. 9. Histogram distribution for 10 different persons in the case of 100 bins

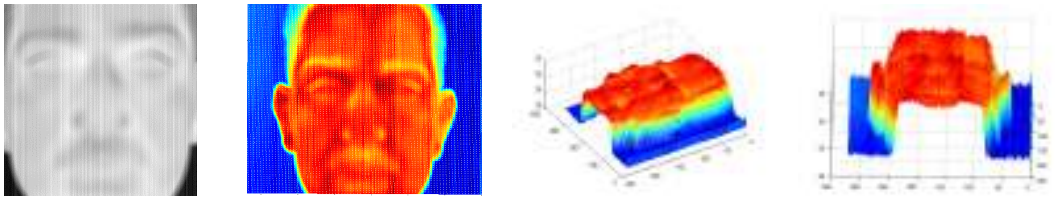

(a) (b) (c) (d)

Fig. 10. (a) A thermal image corresponding to one person, (b) A colour image showing temperature degree distribution of (a), (c) 3D temperature distribution for (a) and (d) another 3D perspective for the same thermal face image

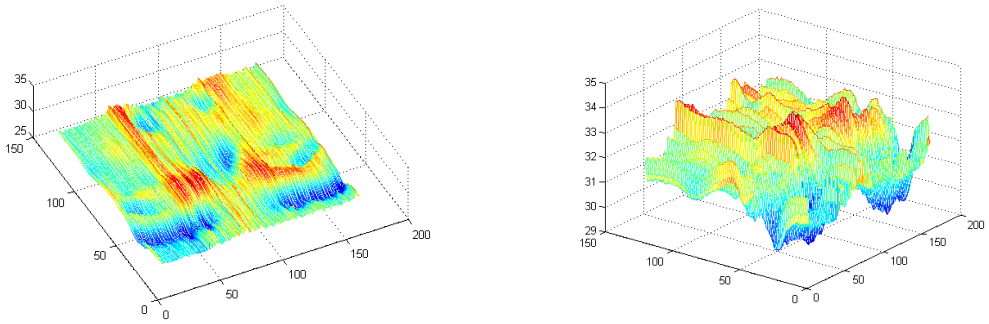

Fig.11. 3D temperature distribution from two angles corresponding to component f_1^0 for the person shown in Fig. 10

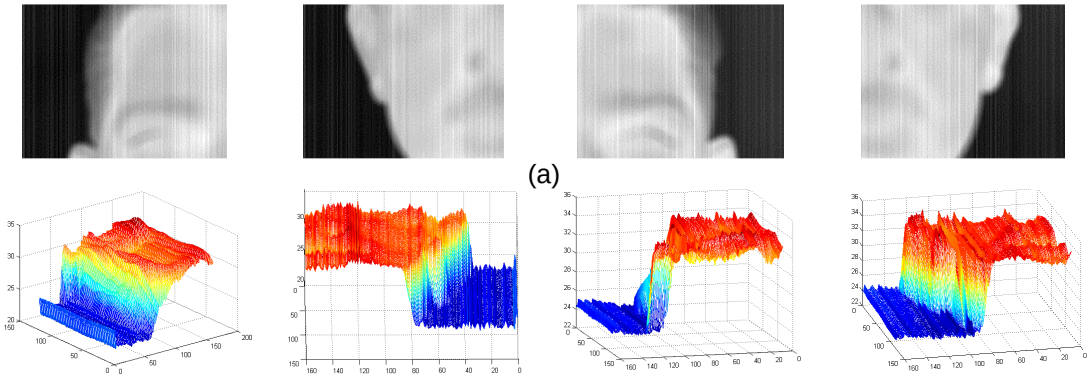

(a)

(b)

Fig. 12. (a) Four thermal image components $f_2^0, f_2^1, f_2^2, f_2^3$ corresponding to person shown in Fig. 10, and (b) the corresponding 3D temperature distributions

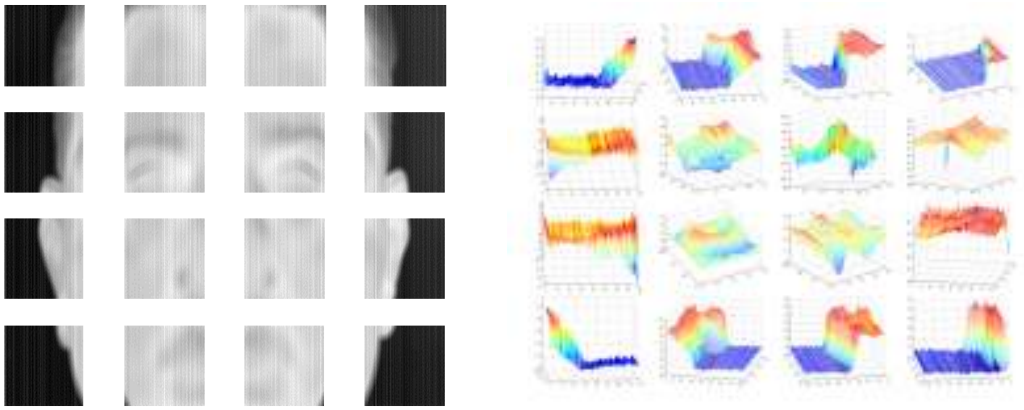

(a)

(b)

Fig. 13. (a) 16 thermal image components $f_3^0, f_3^1, f_3^2, \ldots, f_3^{15}$ corresponding to person shown in Fig. 10, and (b) the corresponding 3D temperature distributions

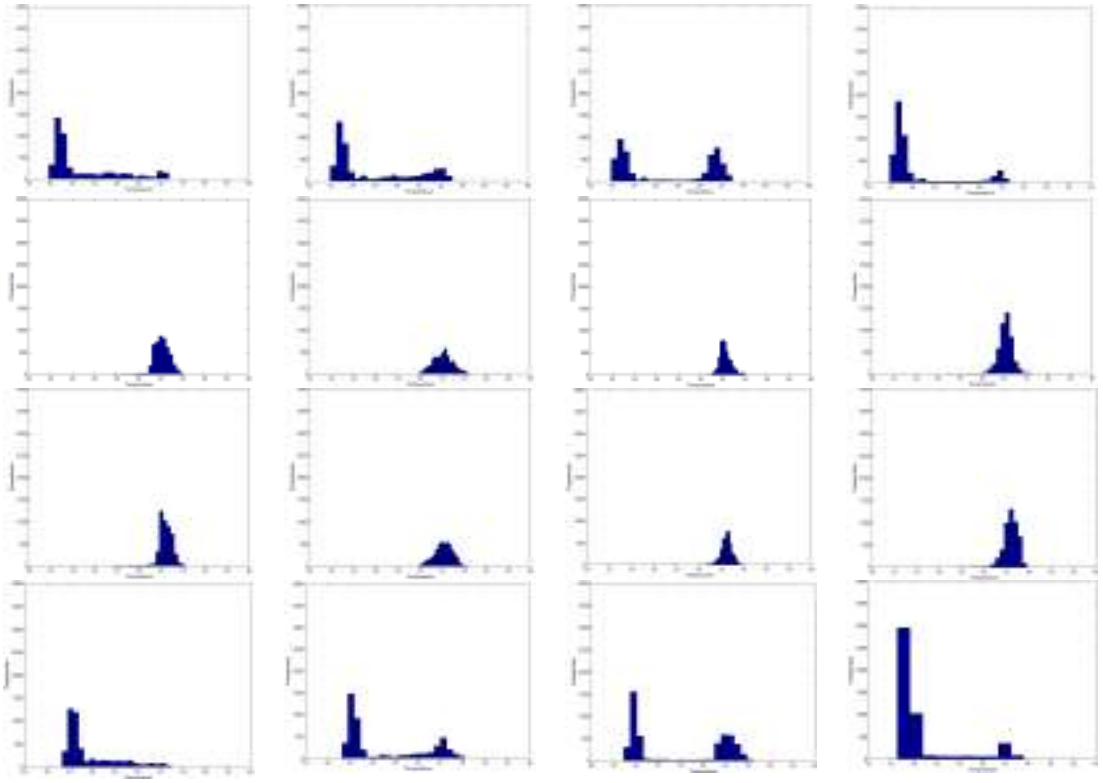

Fig. 14. Histogram distribution for 16 different components $f_3^0, f_3^1, f_3^2, \ldots, f_3^{15}$ corresponding to person shown in Fig. 10

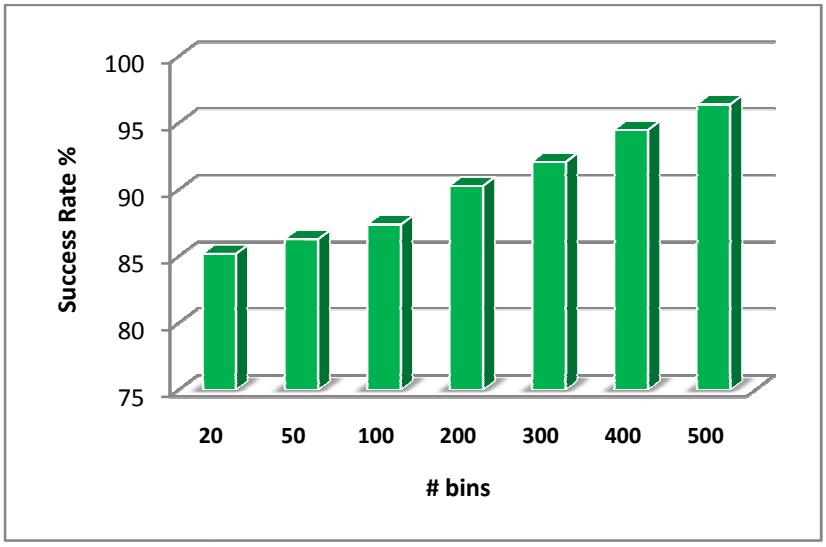

Fig. 15. Recognition rates for different numbers of bins

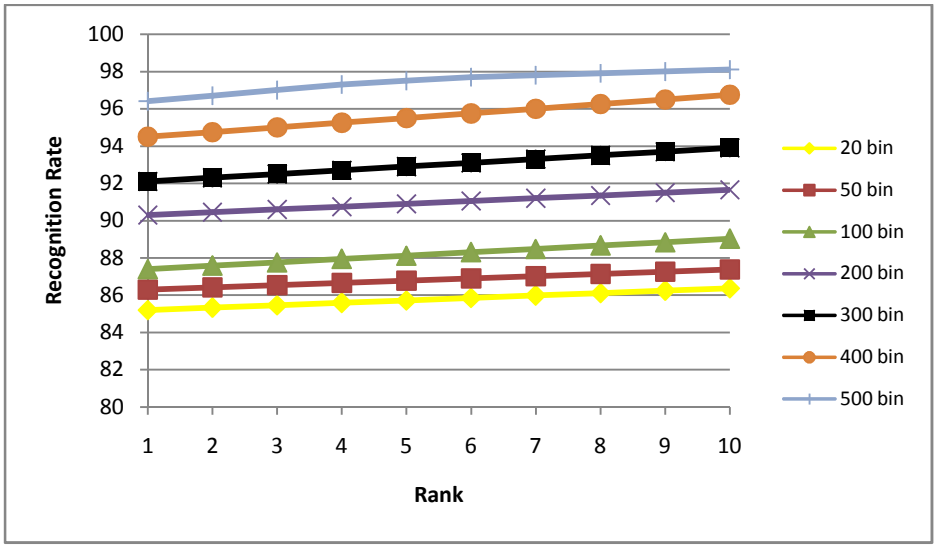

Fig. 16. CMS evaluation results for different numbers of bins

Table 3. Comparison between different thermal face recognition methods proposed in the literature

Method	Success rate (%)
Seal et al. [20]	95
Lu et al. [15]	89.1
Seal et al. [21]	97.6
Bhattacharjee et al. [22]	95.1
Hermosilla et al. [12]	95.7
Socolinsky et al. [10]	93.9
Bhowmik et al. [31]	93.8
Our method	96.4

Table 4. Time consumed (in seconds) to calculate the histogram for the different components for different images of the same subject

	Image 1	Image 2	Image 3	Image 4	Image 5
f_1^0	6.0E-03	6.1E-03	6.0E-03	6.0E-03	5.9E-03
f_2^0	6.2E-03	5.9E-03	6.0E-03	5.9E-03	5.9E-03
f_2^1	5.9E-03	5.9E-03	5.9E-03	6.3E-03	5.9E-03
f_2^2	5.9E-03	5.9E-03	5.9E-03	5.9E-03	6.1E-03
f_2^3	6.0E-03	5.9E-03	6.7E-03	5.9E-03	5.9E-03
f_3^0	5.6E-03	5.6E-03	5.6E-03	5.6E-03	5.6E-03
f_3^1	5.6E-03	5.5E-03	5.6E-03	5.7E-03	5.6E-03
f_3^2	5.6E-03	5.6E-03	5.6E-03	5.6E-03	5.5E-03
f_3^3	5.6E-03	5.6E-03	5.6E-03	5.8E-03	5.6E-03
f_3^4	5.5E-03	5.6E-03	5.6E-03	5.8E-03	5.6E-03
f_3^5	5.6E-03	5.7E-03	5.6E-03	5.6E-03	5.6E-03
f_3^6	5.6E-03	5.6E-03	5.7E-03	5.7E-03	5.7E-03
f_3^7	5.6E-03	5.6E-03	5.6E-03	5.6E-03	5.6E-03
f_3^8	5.6E-03	5.6E-03	5.6E-03	5.6E-03	5.6E-03
f_3^9	5.6E-03	5.6E-03	5.6E-03	5.6E-03	5.7E-03
f_3^{10}	5.6E-03	5.6E-03	5.6E-03	5.7E-03	5.6E-03
f_3^{11}	5.6E-03	5.6E-03	5.6E-03	5.6E-03	5.9E-03
f_3^{12}	5.6E-03	5.6E-03	5.9E-03	5.5E-03	5.7E-03
f_3^{13}	5.6E-03	5.6E-03	5.6E-03	5.6E-03	5.7E-03
f_3^{14}	5.7E-03	5.6E-03	5.6E-03	5.6E-03	5.6E-03
f_3^{15}	5.5E-03	5.6E-03	5.5E-03	5.5E-03	5.8E-03

6. CONCLUSION

Face recognition using different imaging modalities, particularly infrared imaging sensors, has become an area of growing interest. The use of thermal IR images can improve the performance of face recognition in uncontrolled illumination conditions. In this paper, we presented a new technique for face recognition using data fusion based on statistical calculations of component-based thermal images. Local representations offer robustness against variability due to changes in localized regions of the faces. The proposed system exploits the advantages and the characteristics of thermal images, a component-based approach, the statistical features and fusion. The proposed feature vector consists of first moment, second moment and the thermal image histogram, where the calculation of these features is implemented at the component level, beside the whole face image. We have found that the recognition rate increases as the number of histogram bins increases. The best obtained success rate was 96.4% when the number of bins was equal to 500. Our future work will consider implementing the method on larger and benchmark databases.

COMPETING INTERESTS

I declare that there are no competing interests.

REFERENCES

1. Chen X, Flynn PJ, Bowyer K. IR and visible light face recognition. Comput Vis Image Underst. 2005;99:332-358.
2. Zhao W, Chellappa R, Phillips PJ, Rosenfeld A. Face recognition: A literature survey. ACM Computing Surveys (CSUR). 2003;35(4):399-458.
3. Kong SG, Heo J, Boughorbel F, Zheng Y, Abidi BR, Koschan A, et al. Multiscale fusion of visible and thermal IR images for illumination-invariant face recognition. Int J Comput Vis. 2007;71(2):215-233.
4. Yoshitomi Y, Miyaura T, Tomita S, Kimura S. Face identification using thermal image processing. Proc. IEEE Int'l Workshop on Robot and Human Communication. 1997:374-379.
5. Prokoski F. History, current status, and future of infrared identification. Proceedings of IEEE Workshop on Computer Vision beyond the Visible Spectrum: Methods and Applications. 2000:5-14.
6. Wolff LB, Socolinsky DA, Eveland CK (2006). Face recognition in the thermal infrared. In: Bhanu, B, Pavlidis, I, editors. Computer Vision beyond the Visible Spectrum. London: Springer; 2006.
7. Available: http://www.aou.edu.kw
8. San Martin C, Meza P, Torres S, Carrillo R. Improved infrared face identification performance using nonuniformity correction techniques. Lecture Notes on Computer Science. 2008(5259):1115-1123.
9. Socolinsky D, Selinger A. A comparative analysis of face recognition performance with visible and thermal infrared imagery. Proceedings of the 16th International Conference on Pattern Recognition. 2002(4):217-222.
10. Socolinsky D, Selinger A. Thermal face recognition in an operational scenario. Proceedings of IEEE Conference on Computer Vision and Pattern Recognition. 2004(4):187-190.
11. Socolinsky D, Selinger A. Face recognition in the dark. Conf. on Computer Vision and Pattern Recognition Workshop. 2004;18(8):129-134.
12. Hermosilla G, Loncomilla P, Ruiz del Solar J. Thermal face recognition using local interest points and descriptors for HRI applications. 2011:25-35.
13. Akhloufi MA, Bendada A. Probabilistic Bayesian framework for infrared face recognition. World Academy of Science, Engineering and Technology. 2009(60):66-70.
14. Bhowmik MK, Saha K, Majumder S, Majumder G, Saha A, Sarma AN, Bhattacharjee D, Dipak Basu K, Nasipuri M. Thermal infrared face recognition – a biometric identification technique for robust security system. Reviews, Refinements and New Ideas in Face Recognition. ISBN: 978-953-307-368-2, InTech; 2011.
15. Lu Y, Yang J, Wu S, Fang Z, Zhihua Xie. Normalization of infrared facial images under variant ambient temperatures. Advanced Biometric Technologies, ISBN: 978-953-307-487-0, InTech; 2011.
16. Huang X, Lei Z, Fan M, Wang X. Regularized discriminative spectral regression method for heterogeneous face matching. IEEE Trans Image Process. 2013;22(1):353-362.
17. Nicolo F, Schmid NA. Long range cross-spectral face recognition: Matching SWIR against visible light images. IEEE Trans Information Forensics and Security. 2012;7(6):1717-1726.
18. Guzman AM, Goryawala M, Wang J, Barreto A, Andrian J, Rishe N, Adjouadi M. Thermal imaging as a biometrics approach to facial signature authentication. IEEE J Biomed Health Inform. 2013;17(1):214-222.

19. Poursaberi A, Vana J, Mracek S, Dvora R, Yanushkevich SN, Drahansky M, et al. Facial biometrics for situational awareness systems. Biometrics IET. 2013;2(2):35-47.
20. Seal A, Ganguly S, Bhattacharjee D, Nasipuri M, Basu DK. Thermal human face recognition based on Haar wavelet transform and series matching technique. Proceedings of the First International Conference. 2012:155-167.
21. Seal A, Ganguly S, Bhattacharjee D, Nasipuri M, Basu DK. Automated thermal face recognition based on minutiae extraction. International Journal of Computational Intelligence Studies. 2013;2:133-156.
22. Bhattacharjee D, Seal A, Ganguly S, Nasipuri M, Basu DK. A comparative study of human thermal face recognition based on Haar wavelet transform and local binary pattern. ComputIntell Neurosci; 2012. Article ID 261089, doi:10.1155/2012/261089.
23. Akhloufi M, Bendada A. Multispectral infrared face recognition: A comparative study. Tenth International Conference on Quantitative Infra Red Thermography; 2010.
24. Tongzhou Z, Jin L, Zelin A, Nian C, Hui M. New image fusion-based algorithm to face recognition. Third International Conference on Multimedia and Ubiquitous Engineering; 2009.
25. Zaeri N, Kittler J, Cherri A. Efficient component-based face recognition system for high speed devices. International Conference on Design and Architectures for Signal and Image Processing; 2008.
26. Xu Y, Zhang D, Yang J, Yang JY. A two-phase test sample sparse representation method for use with face recognition. IEEE Trans Circuits Syst Vid Tech. 2011;21(9):1255-1262.
27. Xu Y, Zhu Q, Fan Z, Zhang D, Mi J, Lai Z.Using the idea of the sparse representation to perform coarse- to fine-face recognition. Inf Sci. 2013;238:138-148.
28. Yang, J, Zhang, L, Xu, Y, Yang, J. Beyond sparsity: The role of L_1-optimizer in pattern classification. Pattern Recognit. 2012;45:1104-1118.
29. Zaeri N. Discriminant phase component for face recognition. J Electr Comp Eng; 2012. doi:10.1155/2012/718915.
30. Poh N, Kittler J. A unified framework for biometric expert fusion incorporating quality measures. IEEE Trans Pattern Anal Mach Intell. 2012;34(1):3-18.
31. Bhowmik MK, Bhattacharjee D, Basu D K, Nasipuri M. A comparative study on fusion of visual and thermal face images at different pixel level. International Journal of Information Assurance and Security. 2011;6(1):80-86.

Peer-review history:
The peer review history for this paper can be accessed here:
http://www.sciencedomain.org/review-history.php?iid=366&id=5&aid=2846